



## Optimization of total organic carbon removal of a real dyeing wastewater by heterogeneous Fenton using response surface methodology

Bi Gouessé Henri Briton<sup>a</sup>, Laurent Duclaux<sup>b,\*</sup>, Yohan Richardson<sup>c</sup>, Kouassi Benjamin Yao<sup>a</sup>, Laurence Reinert<sup>b</sup>, Yasushi Soneda<sup>d</sup>

<sup>a</sup>Laboratoire de Procédés Industriels de Synthèse, de l'Environnement et des Energies Nouvelles (LAPISEN), Institut National Polytechnique Félix Houphouët Boigny (Côte d'Ivoire), BP 1093 Yamoussoukro

<sup>b</sup>Laboratoire Chimie Moléculaire et Environnement (LCME), Université Savoie Mont Blanc, 73000 Chambéry, France, email: laurent.duclaux@univ-smb.fr (L. Duclaux)

<sup>c</sup>Laboratoire Biomasse Energie et Biocarburants (LBEB), Institut International d'ingénierie de l'eau et de l'Environnement (Burkina Faso), 01 Bp 594 Ouagadougou 01, Burkina Faso

<sup>d</sup>National Institute of Advanced Industrial Science and Technology, Energy Technology Research Institute, 16-1 Onogawa, Tsukuba, Ibaraki 305-8569, Japan

Received 8 March 2018; Accepted 22 July 2018

### ABSTRACT

An iron-activated carbon catalyst was prepared by calcination of an activated carbon derived from banana spike previously impregnated with iron sulphate, and then characterized by N<sub>2</sub> and CO<sub>2</sub> adsorption-desorption experiments and scanning electron microscopy coupled to energy dispersive spectroscopy. The presence of iron-based nanoparticles highly dispersed in the porosity was demonstrated and the nanoparticles were identified as wüstite (FeO) by X-ray photoelectron spectroscopy. The performances of this catalyst were investigated for the treatment of actual textile wastewater from Bamako handicraft loincloths dyeing by the heterogeneous Fenton process. The response surface methodology was used to optimize the effects of three independent parameters (catalyst dose, H<sub>2</sub>O<sub>2</sub> concentration, and initial total organic carbon (TOC) concentration) on the efficiency of wastewater treatment assessed by the rate of TOC reduction. The optimal conditions are found for 2 g/L catalyst, 16.73 mmol/L H<sub>2</sub>O<sub>2</sub> and 99.83 mg/L initial TOC corresponding to a prediction of 90.2% reduction of TOC. In these experimental conditions, the measured rate of degradation of 90.4% is in agreement with the proposed model. This high level of mineralization demonstrates that the Fenton process using the prepared catalyst is a viable treatment for the waste water from Bamako handicraft textile dyeing.

*Keywords:* Activated carbon; Catalyst; Dye; heterogeneous Fenton; Optimization; Wastewater treatment

### 1. Introduction

Handicraft textile dyeing undoubtedly represents an economic sector in the South Saharan countries, notably Mali, because the "Bazin" loincloths resulting from this activity defy any competition on the regional market. This process requires the use of synthetic dyes dissolved in water for the impregnation of white fabric. It thus generates large amounts of wastewater (estimated at 360,000 m<sup>3</sup>/year from the dyeing

shops in Bamako, capital city of Mali), which are discharged directly into the environment without any treatment. This represents a threat of environmental pollution due to the low biodegradability of textile effluents by biological processes [1,2].

Therefore, these textile effluents must be treated though several treatment processes have run up against the removal of dyes which are highly resistant macromolecules. Among the efficient processes, the adsorption on porous materials,

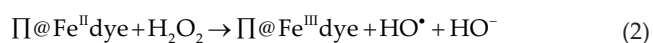
\* Corresponding author.

coagulation, chlorination and ultrafiltration can be mentioned [3,4]. However, for these methods, pollutants have only been transferred from the aqueous phase to the solid one, thus creating a secondary contamination.

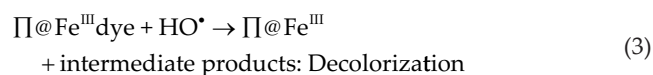
Thus, advanced oxidation processes (AOP) such as photocatalytic degradation, catalytic ozonation, electrochemical oxidation and Fenton processes [5] have been successfully developed to degrade compounds of different and complex chemical structures [6]. Although these AOP are effective to degrade refractory pollutants in textile wastewater, they remain limited for the treatment of heavily loaded effluents with chemical oxygen demand (COD) between 10 and 100 g/L, due to clogging of active sites generating radical species [7]. In addition, a high pollutant concentration reduces the penetration of ultraviolet radiation and hinders the processing of heterogeneous photocatalysis. Despite wet air oxidation (catalyzed or not) is very promising for the treatment of such effluents [8], this process is carried out at temperatures up to 300°C and at extremely high pressures up to 20 MPa in the presence of pure dioxygen [7,8], implying prohibitive investment and operating costs. In addition, as the mineralization remains partial in this process, the refractory compounds need to be further biologically degraded [9].

Otherwise, these highly charged effluents can be treated with environmentally friendly processes such as the Fenton process with a prior dilution [10,11] to avoid the clogging of active sites. Indeed, the heterogeneous Fenton process has proved its high efficiency in degrading the recalcitrant compounds under mild conditions with the hydroxyl radicals generated through the reaction between the iron active species at the catalyst surface and hydrogen peroxide. The high reactivity of the heterogeneous Fenton process has been reported at reaction temperatures around 30°C and in a wide range of pH values, overcoming one of the main limitations of the classical homogeneous process [12,13].

Besides, if supported catalysts are used, the surface of the support materials is also capable of fixing the target pollutants by adsorption at the vicinity of the active sites generating hydroxyl radicals. Thus, efforts are increasingly carried out to develop porous materials [14] (referred to “Π”) with iron oxide nanoparticles well dispersed and strongly tied to the support. For this purpose, several porous materials, such as silica [15], zeolite [16], bentonite [17], activated carbon [18], have been used to disperse the iron oxide nanoparticles within the pores. In these kinds of iron oxide supported catalysts, the reaction mechanism of the heterogeneous Fenton degradation of dye is known to occur for instance, as follows [19–21]:



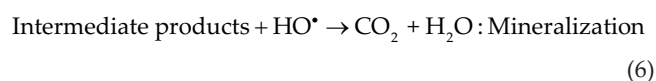
After an adsorption stage of the dye on the porous support (Eq. (1)) and the generation of hydroxyl radicals at the surface of the catalyst (Eq. (2)), the radicals  $HO^\bullet$  attack primarily the chromophoric groups responsible for the color of the dyes to transform them into intermediate compounds (Eq. (3)):



Fe(III) is reduced by  $H_2O_2$  to highly reactive Fe(II) followed by the production of hydroxyl radicals (Eq. (4)). Fe(II) is also oxidized by  $H_2O_2$  to Fe(III) followed by the production of hydroxyl radicals (Eq. (5)):



The mineralization of intermediate compounds in  $CO_2$  and  $H_2O$  is much slower because of the presence of very resistant aromatic rings [19] (Eq. (6)).



Activated carbon has properties such as high surface area, wide porosity range and surface functional groups making it a favorite catalytic support in the Fenton oxidation process [22,23]. The presence of micropores and mesopores promotes a good dispersion of the nanoparticles of iron oxide and prevents their agglomeration during their growth [24]. In fact, the iron oxide nanoparticles' agglomeration in the pores might also hinder the adsorption of the target pollutants on the active sites where the hydroxyl radicals operate [25]. Thus, for operating Fenton oxidation processes, the importance of dispersion of the iron nanoparticles within the pores of micro-mesoporous activated carbons has been reported by several studies [26,27]. Such a catalytic support with wide pore distribution is generally obtained by the chemical activation of lignocellulosic biomasses from abundant agricultural waste [28].

Despite their catalytic potential, the iron oxide nanoparticles supported on activated carbon are very rarely used for the treatment of real wastewater. However, some authors have achieved very efficient wastewater treatment as the optimal conditions were found [27,29]. These results have been obtained according to a conventional multifactorial experimental approach which has proved to be time consuming and expensive. This classical experiment does not allow to evaluate the interaction effects between the different independent variables involved in wastewater treatment and thus usually leads to a partial conclusion [30]. Thus, the response surface methodology (RSM) can be used to search for optimal conditions for treating real wastewater [31,32]. RSM is a statistical tool for designing experiments, evaluating the individual effects of independent variables and their interactions, statistical modeling and process optimization with a limited number of experiments [33]. RSM often uses the central composite design (CCD) as an experimental model to build a model which can be fitted by the least squares technique [34].

To our knowledge, the statistical optimization for the search of optimal treatment conditions of a real textile wastewater by the heterogeneous Fenton process using iron nanoparticles supported on activated carbon has not yet been

reported. In this work, RSM was used to design, model and optimize the effects of three main independent parameters (catalyst dose,  $\text{H}_2\text{O}_2$  concentration and initial total organic carbon (TOC) concentration) on the degradation of refractory organic compounds present in a real textile effluent from Bamako. For this purpose, a heterogeneous catalyst consisting of iron oxide nanoparticles supported on a micro and mesoporous activated carbon was prepared from banana spike. The prepared supported catalyst has been used for the treatment of a dyeing wastewater by using the heterogeneous Fenton process in batch reactors. The degradation of organic compounds has been studied in terms of TOC removal efficiency. In addition, the TOC removal kinetics as well as the stability and reusability of the catalyst have been studied.

## 2. Materials and methods

### 2.1. Chemicals

The reagents used were all of analytical grade:  $\text{H}_2\text{O}_2$  (35 wt%, Sigma-Aldrich, Saint-Quentin-Fallavier, France); iron sulfate  $\text{FeSO}_4 \cdot 7\text{H}_2\text{O}$  (99.5%, Merck, Saint Quentin-Fallavier, France); NaOH (0.1 mol/L, Sigma-Aldrich),  $\text{Na}_2\text{SO}_3$  (>99%, Sigma-Aldrich), HCl (37 wt%, Sigma-Aldrich) and  $\text{H}_3\text{PO}_4$  (85 wt%, Sigma-Aldrich).

### 2.2. Preparation and characterization of the heterogeneous catalyst

The spike of banana is a lignocellulosic biomass feedstock that can be used to produce activated carbon because it contains about 21.23 wt% hemicellulose, 19.06 wt% lignin, and then 41.75 wt% carbon [35]. First of all, spikes of the banana bunch from Ivory Coast were washed with distilled water to eliminate the impurities and dried at  $105^\circ\text{C}$  for 24 h prior to their activation. Dried and crushed precursor was chemically activated by impregnation with phosphoric acid at a ratio of  $3.34/1$  ( $m_{\text{H}_3\text{PO}_4} / m_{\text{precursor}}$ ). After impregnation, the mixture was filtered to recover the solid residue which was dried in an oven at  $50^\circ\text{C}$  for 72 h. Then, a weighted amount of impregnated precursor was heated in a muffle furnace (heating rate of  $10^\circ\text{C}/\text{min}$ ) at  $480^\circ\text{C}$  for 2 h. The obtained activated carbon was washed several times with distilled water to eliminate the excess of acid and then dried in a desiccator.

The heterogeneous catalyst was subsequently prepared by wet impregnation of 4 g of activated carbon (impregnation ratio of 11% Fe mass/mass) carried out in 200 mL of distilled water containing 2.215 g Fe/L from iron sulphate ( $\text{FeSO}_4 \cdot 7\text{H}_2\text{O}$ ). After magnetic stirring for 2 h at 300 rpm to adsorb the iron ions, the solid was dried using a rotavapor, calcined for 2 h at  $350^\circ\text{C}$  and cooled in a desiccator before being finely crushed and sieved to produce catalyst particles of sizes smaller than  $125 \mu\text{m}$  and labeled AC@Fe.

The textural characteristics of the catalyst have been determined by using an automatic sorptometer (ASAP2020, Micromeritics, Merignac, France) and compared with the ones of the activated carbon. Prior to measurements, samples have been degassed for 12 h at 523 K under vacuum.  $\text{N}_2$  adsorption-desorption isotherms and  $\text{CO}_2$  adsorption isotherms have been measured at 77 and 273 K, respectively. BET (Brunauer–Emmett–Teller) specific surface areas have been calculated from the  $\text{N}_2$  isotherms in the relative pressure range 0.01–0.05. The pore size distributions (PSD) have been determined by

using NLDFIT (non-local density functional theory) slit pore models applied on both the  $\text{N}_2$  and  $\text{CO}_2$  isotherms.

The chemical elements have been mapped using a ZEISS ULTRA 55 Gemini field emission gun scanning electron microscope (FEG-SEM) coupled to an EDAX-type energy dispersive spectrometer (EDS). The iron dose in AC@Fe was determined by calcining and etching the ash in a solution of 5 mL concentrated HCl (37% wt). Then 20 mL of distilled water were added to the mixture and boiled up to 1/3 of the volume. After cooling, the solution was filtered on paper and its volume was extended to 50 mL with distilled water and then analyzed with the Varian SpectraAA20 spectrometer using the atomic absorption method. The Fe2p spectra and the mass content of the chemical elements have been determined by X-ray photoelectron spectroscopy (XPS) using an ESCALab 220i-XL spectrometer (Fisons Instruments, Arcueil, France), equipped with an Al K $\alpha$  monochromatic source and a hemispherical analyzer.

### 2.3. Textile wastewater and analytical procedures

The wastewater sample was collected in a tank receiving the effluents from a textile dyeing craft firm in Bamako. This effluent is composed of a mixture of organic dyes (indigo, turquoise blue, etc.) used to dye multicolored loincloths, sodium hydroxide (NaOH), sodium hydrosulfite ( $\text{Na}_2\text{S}_2\text{O}_4$ ), copper sulfate ( $\text{CuSO}_4$ ) and starch.

The COD ( $\text{mg O}_2/\text{L}$ ) was determined by titration of the excess of potassium dichromate with an ammonium iron sulfate solution in the presence of ferroin after hot oxidation of the organic matter in sulfuric acid medium. The biochemical oxygen demand (BOD,  $\text{mgO}_2/\text{L}$ ) was determined according to the respirometric BOD OxiTop method [36]. The TOC ( $\text{mgC}/\text{L}$ ) concentration was determined by a “Shimadzu TOC-V<sub>CSN</sub>” analyzing instrument using a potassium phthalate solution as calibration standard. TOC was determined by subtracting the total inorganic carbon (TIC) from the total carbon (TC). Indeed, the sample is introduced into the combustion reactor at  $680^\circ\text{C}$  using a syringe. In the presence of dioxygen and platinum catalyst, the carbon fraction is completely converted to  $\text{CO}_2$ . After cooling, drying and purification, the  $\text{CO}_2$  is measured by the non-dispersive infra red (NDIR) in peak form. TC is obtained by comparison with a calibration performed under the same conditions. Finally, a new test portion is subjected to HCl (2 N) acid attack to eventually convert the carbonate or bicarbonate ions into  $\text{CO}_2$  which is sent to the NDIR detector to determine the sample TIC. The spectral variation of the dissolved organic compounds in the raw and in the treated effluents was obtained by a UV-visible absorption spectrometer (Cary scan 50 mark). The characteristics of the collected effluent are COD = 24,210  $\text{mgO}_2/\text{L}$ ; BOD = 3,748  $\text{mgO}_2/\text{L}$ ; TOC = 10,720  $\text{mgC}/\text{L}$  and pH = 11.7. BOD/COD ratio lower than 0.2, confirms that this textile effluent is not biodegradable [29]. The UV-visible spectrum of the effluent has shown three peaks of maximum absorption at 283, 260 and 227 nm, revealing the presence of benzene rings [37].

### 2.4. Experimental procedures for treatment of textile wastewater

The degradation tests were carried out in 100 mL stoppered Pyrex vials, each containing 50 mL of textile wastewater. The pH of the samples diluted according to a given

TOC dose (53.25–214.4 mgC/L) corresponding to the experimental design were reduced to  $4.02 \pm 0.01$  by addition of 0.1 mol/L HCl. After addition of a weighted amount of catalyst (0.4–2.0 g/L), the mixtures were agitated for 2 min at 250 rpm in an orbital shaker for a homogeneous dispersion. The vials were maintained in the shaker for 30 min at 32°C to match the working temperature conditions (similar to average ambient temperature expected in Mali). Then, the Fenton reaction was initiated by addition of H<sub>2</sub>O<sub>2</sub> (8.1–30.3 mmol/L) in the vials further shaken at 250 rpm for 15 h. After this reaction time, 0.3 mL of a 0.1 M NaOH/0.25 M Na<sub>2</sub>SO<sub>3</sub> solution was added to each flask to stop the Fenton reaction by deactivation of the hydroxyl radicals and to precipitate the dissolved iron ions. The reaction mixtures were filtered using a syringe filter (HVLP-type Millipore filter  $\phi = 0.45 \mu\text{m}$ ) and the TOC concentrations of the filtrates were measured. The efficiency of the degradation process has been evaluated by the determination of the TOC reduction rate (Y %), according to Eq. (7):

$$Y(\%) = \left(1 - \frac{C}{C_0}\right) \times 100 \tag{7}$$

where C<sub>0</sub> and C represent the TOC concentration of the wastewater sample measured initially and after 15 h of Fenton reaction, respectively.

All these TOC reduction tests were realized according to the RSM to find the optimal treatment conditions. After validation of the optimal conditions predicted by the model, the stability of the AC@Fe catalyst was studied. Finally, the biodegradability potential of this textile wastewater treated by the heterogeneous Fenton process using AC@Fe under optimal conditions was evaluated by BOD/COD ratio, average oxidation state (AOS) and carbon oxidation state (COS) indices.

### 2.5. Experimental design

The response surface methodology (RSM) using the CCD was used to search for the optimal degradation conditions of the organic pollutants contained in this wastewater. The RSM is a set of mathematical and statistical techniques for the design of experiments, the modeling and the evaluation of the effects of experimental factors [38]. This approach allows evaluating the factors that affect the TOC concentration abatement and the interactions between them. According to the literature, five independent variables namely the pH, the temperature, the amount of hydrogen peroxide, the concentration of the pollutant and the amount of catalyst, influence the Fenton process [39]. Previous works have shown that the heterogeneous Fenton reaction is effective at pH = 4, and at a temperature of 30°C [37]. Actually, at pH values lower than 4, the process is very effective, but generates a leaching of iron in the solution [40]. It should also be noted that the average temperature of the textile effluents in Bamako is close to 30°C. Thus, three variables, which are the amount of AC@Fe, the H<sub>2</sub>O<sub>2</sub> dose and the initial TOC concentration have been chosen to search for the optimal conditions. The H<sub>2</sub>O<sub>2</sub> dose has been varied in the 8.1–30.3 mmol/L range and the TOC rate in the 53.25–214.4 mg/L range, in

agreement with the stoichiometry of the reduction of the COD (1 g COD = 0.03125 mol dioxygen corresponding to 0.0625 mol H<sub>2</sub>O<sub>2</sub>) [41].

The number of tests to be performed defined by the CCD consists of 2<sup>k</sup> factorial tests, 2k axial tests and n<sub>c</sub> central tests. The central tests are useful to determine the experimental error and the reproducibility of the data. As “k” is the number of factors or independent variables (i.e., 3, see above), 20 tests have been carried out, including six central tests. The independent variables are coded in the (–1, 1) interval. Low and high previously defined levels are coded –1 and +1, respectively. The axial points are located at (±α, 0, 0), (0, ±α, 0) and (0, 0, ±α) where α represents the distance from each point to the axial center and acts for the rotary design. In this study, the α value was set at 1.682 (rotary) [42]. The ranges and the levels of the studied variables are given in Table 1.

To compare different variables of various units and for statistical calculations, the variables x<sub>i</sub> were coded as X<sub>i</sub> according to the following equation (Eq. (8)):

$$X_i = \frac{x_i - x_0}{\delta x} \tag{8}$$

where x<sub>0</sub> is the value of x<sub>i</sub> at the center point and δx represents the step change [43].

The degradation of the organic compounds during the Fenton treatment has been assessed by the TOC rate reduction representing the Y response in percentage.

The results of the different tests (i.e., the response) have been modeled by a second degree polynomial equation as follows:

$$Y = b_0 + \sum_i b_i X_i + \sum_i b_{ii} X_i^2 + \sum_i \sum_j b_{ij} X_i X_j \tag{9}$$

where Y is the predicted response; b<sub>0</sub> is a constant coefficient; b<sub>i</sub> are linear coefficients; b<sub>ij</sub> are interaction coefficients; b<sub>ii</sub> are quadratic coefficients and X<sub>i</sub> and X<sub>j</sub> are the coded values of the variables.

The “Statgraphics Centurion XVI” software [44] was used to establish the quadratic regression equation using the ordinary least squares method to plot the curves of response surface and curves of isoresponse, and then, to optimize the treatment conditions. The quality of the fit was judged by the R<sup>2</sup> coefficient of determination and adjusted R<sup>2</sup>. The R<sup>2</sup> coefficient gives the proportion of the total variation of the response predicted by the model, indicating the ratio between the sum of squares due to the regression and the total sum of

Table 1  
Levels of the independent variables in the CCD statistical experiment

Actual variables (x <sub>i</sub> )	Units	Coded variables levels X <sub>i</sub>				
		–1.682	–1	0	1	1.682
AC@Fe: x <sub>1</sub>	g/L	0.4	0.72	1.2	1.68	2
H <sub>2</sub> O <sub>2</sub> : x <sub>2</sub>	mmol/L	8.1	12.6	19.2	25.8	30.3
TOC: x <sub>3</sub>	mg/L	53.25	83.69	135.7	179.25	214.4

squares. A high  $R^2$  coefficient ensures a satisfactory fit of the quadratic model to the experimental data. The coefficient of variation (CV), which represents the percentage ratio of the standard deviation to the mean value, was used to assess the reliability and reproducibility of the model. The results were analyzed statistically by the analysis of variance (ANOVA). To judge the significance of the model as well as each model term, Fisher value ( $F$ -value) and probability value ( $p$ -value) were applied.

### 3. Results and discussion

#### 3.1. Characteristics of AC@Fe catalyst

Inset of Fig. 1 shows that the adsorption–desorption isotherms of nitrogen at 77 K are type IV according to the IUPAC classification [45]. They are typical of both microporous (pore diameter < 2 nm) and mesoporous (2 nm < pore diameter < 50 nm) materials. In addition, the presence of hysteresis loop confirms the mesoporosity of these two materials. Indeed, at relative pressures greater than 0.1, the progressive filling of the mesopores is marked by an evolutionary slope up to 0.995. The hysteresis loop formed by the desorption curve of the nitrogen condensed by capillary action and the curve of adsorption is of H3 type according to the classification of IUPAC suggesting the occurrence of slit-like meso pores [45].

Comparison of the PSD of AC@Fe to the AC one (Fig. 1) confirms that particles might be located in the pores of the

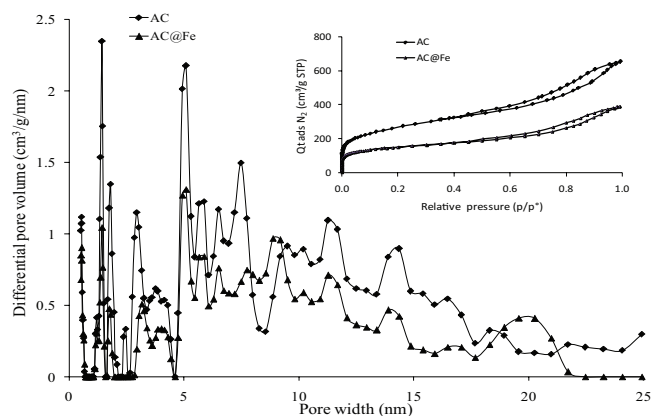


Fig. 1.  $N_2$  pore size distributions of the AC activated carbon (diamond) and the AC@Fe catalyst (triangle). Inset shows  $N_2$  adsorption–desorption isotherm at 77 K of the AC activated carbon and the AC@Fe catalyst.

catalyst. The pores have not been fully blocked by the iron-based nanoparticles as micropores and mesopores are still observed in AC@Fe. As a consequence, the total porous volume of the AC support (i.e., 0.886  $cm^3/g$ ) was reduced to 0.509  $cm^3/g$  after impregnation (Table 2). Moreover, the presence of iron particles in the pores of the AC support has contributed to the reduction of the specific surface area from 896 to 532  $m^2/g$ . However, this specific surface area (532  $m^2/g$ ) of the catalyst is relatively high to promote the degradation of pollutants by the hydroxyl radicals after being adsorbed near the active sites.

The SEM images and the EDS mappings (Fig. 2) have indicated the presence of iron and sulfur on the surface of the supported catalyst already containing carbon, oxygen and phosphorus. These EDS maps indicate that iron atoms (Fig. 2(c)) and sulphur atoms (Fig. 2(d)), are dispersed homogeneously. These iron-based and sulphur-based particles are certainly responsible for the decrease in the specific surface area and the pore volume. In addition, Figs. 2(b) and (c), reveal that the iron and oxygen atoms coexist. This sustains that the iron oxide nanoparticles are formed on the AC support inside the porosity after impregnation and calcination. The formation of iron oxides is due to the nucleophilic nature of oxygen which can easily give electron doublets to the iron ions to form chemical bonds [46,47].

The XPS has allowed quantifying the mass composition of these chemical elements (Table 2) on the external surface of the catalyst. The carbon and phosphorus contents have decreased slightly from 78.61% to 71.25%, and 6.89% to 5.29%, respectively, in the catalyst compared with raw activated carbon due to the presence of iron sulfate decomposition products. Only 2.45% of iron was detected by XPS. This content is relatively lower than the 3.3% iron content obtained by the atomic absorption spectrometry after calcination of AC@Fe. This result agrees with the work of Maneechakr and Karnjanakom [48] who reported that the activated carbon has a low adsorption capacity of iron ions and that part of iron has been occluded in the pores of the activated carbon. Previous works have also shown that the decrease in the porosity and specific surface area of the material was related to the formation of iron nanoparticles ( $Fe_2O_3$ ,  $Fe_3O_4$ ,  $Fe(OOH)$ ,  $FeO$ ) [49,50] during the thermal decomposition of the precursor in an inert atmosphere. The  $Fe2p_{3/2}$  and  $Fe2p_{1/2}$  peaks (located at 711.7 and 724.76 eV, respectively) have been analyzed to identify the nature of the iron oxide in the catalyst matrix (Fig. 3). The  $Fe2p_{3/2}$  signal exhibits a satellite peak centered at 715.72 eV, indicating the presence of wüstite ( $FeO$ ) in agreement with the literature [51,52].

Table 2  
Characterization of the activated carbon (AC) and the supported catalyst (AC@Fe)

Sample	Textural characteristics					Chemical elements (%wt) detected by XPS				
	$V_{ultramicro}$ ( $cm^3/g$ )	$V_{supermicro}$ ( $cm^3/g$ )	$V_{meso}$ ( $cm^3/g$ )	$V_{total}$ ( $cm^3/g$ )	$S_{BET}$ ( $m^2/g$ )	C	O	P	Fe	S
AC	0.159	0.195	0.691	0.886	896	78.61	14.51	6.89	–	–
AC@Fe	0.135	0.083	0.426	0.509	532	71.25	15.46	5.29	2.45	5.55

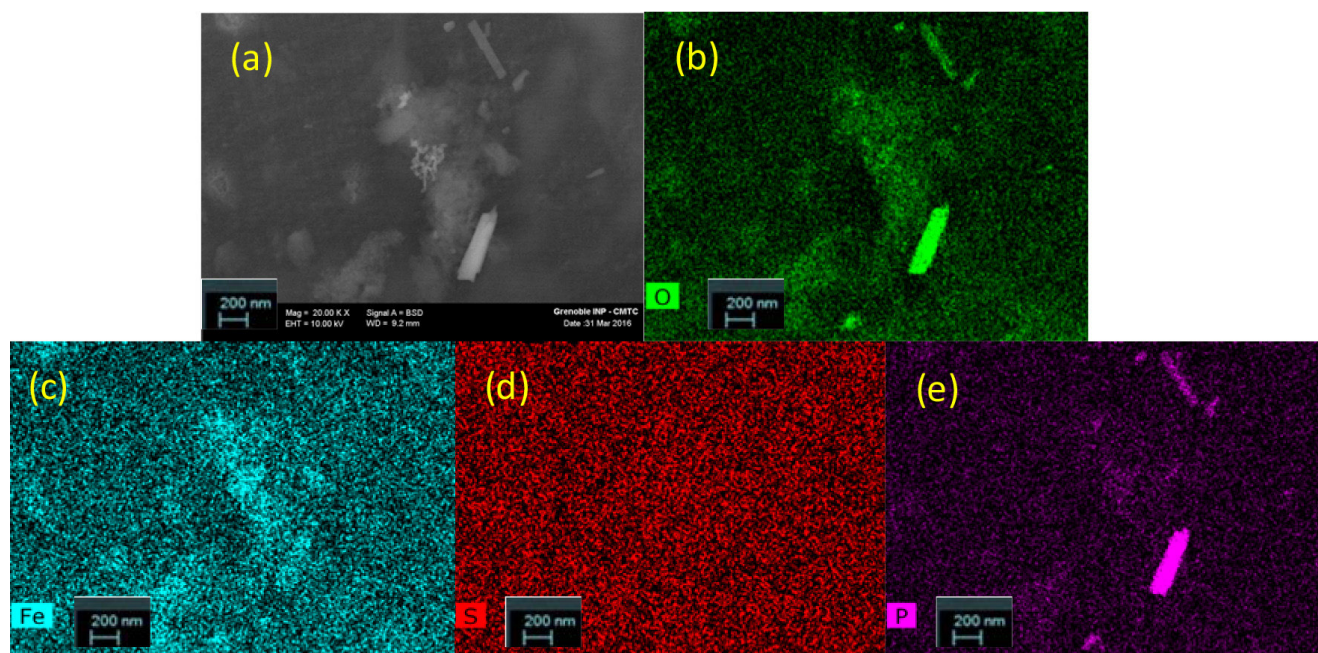


Fig. 2. SEM image of catalyst AC@Fe (a) and corresponding EDS maps of the chemical elements: oxygen (b), iron (c), sulfur (d) and phosphorus (e).

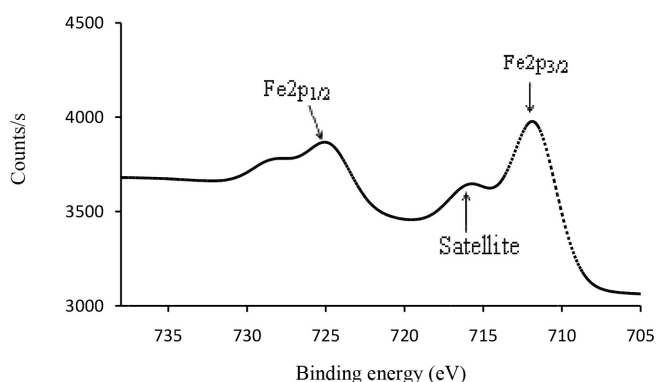


Fig. 3. Fe2p spectrum XPS of the AC@Fe catalyst.

### 3.2. Development of regression model equation and statistical analysis

The experiments carried out on the basis of the three independent variables (catalyst dose:  $X_1$ , dose of  $H_2O_2$ :  $X_2$  and initial concentration of TOC:  $X_3$ ) made it possible to obtain different responses according to the experimental conditions defined by the matrix of the central composite design (Table 3). These experimental conditions and their responses (removal of TOC referred to as  $Y$ ) are reported in Table 3.

Using multiple regression analysis, the elimination of TOC ( $Y$ ) was correlated with the three independent variables. This quadratic regression model chosen for the removal of TOC is represented by the second order polynomial equation (Eq. (10)):

$$Y = 77.27 + 11.41X_1 + 3.74X_2 - 6.34X_3 - 2.79X_1^2 - 2.51X_1X_2 + 1.32X_1X_3 - 1.54X_2^2 + 0.88X_2X_3 - 2.97X_3^2 \quad (10)$$

where  $X_1$ ,  $X_2$  and  $X_3$  are the coded values of the catalyst dose, the  $H_2O_2$  dose and the initial TOC concentration, respectively.

The coefficients of the model equation and their statistical significance were evaluated using the Statgraphics Centurion XVI software. A positive sign in front of the terms indicates a synergistic effect, while a negative sign indicates an antagonistic effect.

Fitting parameter values:  $R^2 = 0.9751$  and  $\text{adj-}R^2 = 0.9528$  indicate that predicted values and experimental values are in good agreement. Indeed, the model was considered valid because the criteria  $R^2 > 0.8$  was satisfied [53]. Moreover, 97.51% of the TOC abatement variations are justified by the independent variables, and the low value of the coefficient of variation ( $CV = 3.67\%$ ) reflects the reliability and reproducibility of the experiments as a model is assumed to be reasonably repeatable if its CV value is less than 10% [54]. Variables such as the catalyst dose and the  $H_2O_2$  dose have a synergistic effect while the initial TOC concentration has an antagonistic effect on the response.

The statistical test of the model has been achieved by analysis of variance (ANOVA, Table 4).  $F$ -value was defined as the ratio of the mean squares of the model and mean square of residual errors. The  $F$ -value calculated is 43.60, which is significantly higher than the tabulated value of Fisher-Snedecor ( $F_p = 3.13$ ) at the 5% significant level. This result demonstrates that the model is valid and robust [55]. The independent variables and the interaction effects are assumed to be statistically significant if the critical probability of each of them is less than 0.05 ( $p$ -value  $< 0.05$ ). Thus, in this study, the variables referred to:  $X_1, X_2, X_3, X_1^2, X_1X_2, X_3^2$  are significant while  $X_2^2, X_1X_3, X_2X_3$  are insignificant on the TOC concentration abatement ( $Y$ ). This shows that the  $X_1, X_2$  and  $X_3$  factors have an established influence on the degradation performance of the organic pollutants in the studied

Table 3  
Results of the central composite design of the TOC reduction

Runs	Coded variables			AC@Fe (g/L)	H <sub>2</sub> O <sub>2</sub> (mmol/L)	TOC (mg/L)	Y <sub>exp</sub> (%)	Y <sub>pred</sub> (%)
	X <sub>1</sub>	X <sub>2</sub>	X <sub>3</sub>					
1	-1	-1	-1	0.72	12.6	83.69	59.21	60.86
2	1	-1	-1	1.68	12.6	83.69	84.8	86.06
3	-1	1	-1	0.72	25.8	83.69	68.94	71.60
4	1	1	-1	1.68	25.8	83.69	87.62	86.74
5	-1	-1	1	0.72	12.6	179.25	43.57	43.77
6	1	-1	1	1.68	12.6	179.25	77.6	74.26
7	-1	1	1	0.72	25.8	179.25	59.97	58.03
8	1	1	1	1.68	25.8	179.25	80.8	78.47
9	-1.682	0	0	0.4	19.2	135.7	52.06	50.20
10	1.682	0	0	2	19.2	135.7	85.75	88.57
11	0	-1.682	0	1.2	8.1	135.7	66.82	66.63
12	0	1.682	0	1.2	30.3	135.7	78.05	79.20
13	0	0	-1.682	1.2	19.2	53.25	82.65	79.53
14	0	0	1.682	1.2	19.2	214.4	54.13	58.21
15	0	0	0	1.2	19.2	135.7	77.58	77.27
16	0	0	0	1.2	19.2	135.7	77.44	77.27
17	0	0	0	1.2	19.2	135.7	77.15	77.27
18	0	0	0	1.2	19.2	135.7	77.39	77.27
19	0	0	0	1.2	19.2	135.7	77.22	77.27
20	0	0	0	1.2	19.2	135.7	76.98	77.27

Table 4  
ANOVA of the quadratic model for TOC reduction

Source	Sum of squares	Degree of freedom	Mean square	F -value	P-value	Remark
Model	2,820.26	9	313.36	43.60	<0.0001	Significant
X <sub>1</sub> : AC@Fe	1,777.16	1	1,777.16	247.24	<0.0001	Significant
X <sub>2</sub> : H <sub>2</sub> O <sub>2</sub>	190.73	1	190.73	26.53	0.0004	Significant
X <sub>3</sub> : TOC	549.08	1	549.08	76.39	<0.0001	Significant
X <sub>1</sub> <sup>2</sup>	111.86	1	111.86	15.56	0.0028	Significant
X <sub>1</sub> X <sub>2</sub>	50.55	1	50.55	7.03	0.0242	Significant
X <sub>1</sub> X <sub>3</sub>	14.02	1	14.02	1.95	0.1928	
X <sub>2</sub> <sup>2</sup>	34.09	1	34.09	4.74	0.0545	
X <sub>2</sub> X <sub>3</sub>	6.21	1	6.21	0.86	0.3744	
X <sub>3</sub> <sup>2</sup>	126.96	1	126.96	17.66	0.0018	Significant
Total error	71.88	10	7.19			
Total (corr.)	2,892.13	19				

wastewater. Therefore, this regression model can be used to predict the treatment of this effluent.

Moreover, the importance of all these factors (variables) observed through ANOVA, as well as their interactions, was highlighted using graphical Pareto analysis. The contribution ( $P_i$ ) of each factor or variable was calculated according to the following relation [56]:

$$P_i = \left( \frac{b_i^2}{\sum b_i^2} \right) * 100 \quad (i \neq 0) \quad (11)$$

where  $b_i$  represents the coefficients of each principal variable  $i$ , their interaction and quadratic effect in Eq. (10).

The Pareto plot (Fig. 4) revealed that the main factors such as the catalyst dose ( $X_1$ ), the dose of H<sub>2</sub>O<sub>2</sub> ( $X_2$ ) and the initial concentration TOC ( $X_3$ ) contributed 61.36%, 6.59% and 18.94%, respectively, for the TOC reduction rate. For quadratic effects, relatively small contributions were found for  $X_1^2$  (3.67%) and  $X_3^2$  (4.16%), while that of  $X_2^2$  (1.12%) is very negligible. These negligible contributions were also obtained for the interaction factors  $X_1X_3$  (0.82%),  $X_2X_3$  (0.36%) and a little more for  $X_1X_2$  (2.97%). As can be seen, catalyst dose is

the most influential factor on the TOC removal efficiency of the textile effluent.

3.2.1. Effect of variables and search for optimal conditions

According to Eq. (10) of the regression model, the rate of reduction of TOC increases together with the amounts of AC@Fe ( $X_1$ ) and  $H_2O_2$  ( $X_2$ ). On the other hand, an increase in the initial concentration of TOC ( $X_3$ ) decreases the efficiency of the heterogeneous Fenton process. In addition to the individual effects of these three factors, the interactive and quadratic effects have to be taken into account in the TOC rate reduction process. A better interpretation requires the analysis of the curves of isoresponses and response surfaces which can locate the optimal areas of the TOC rate reduction.

Fig. 5 shows that the rate of TOC reduction is rapidly evolving with the amount of catalyst to reach more than 80%, whatever the  $H_2O_2$  concentration. According to the contour plot, low amounts of  $H_2O_2$  ( $X_2 < 0$ , less than 19.2 mM) must be offset by high amounts of catalyst. This will provide the  $H_2O_2$  molecules an easy access to the active sites consisting of iron nanoparticles, in order to generate the  $HO^\bullet$  radicals. By increasing the amounts of  $H_2O_2$ , the process is less efficient when the  $X_1$  coded value of the catalyst dose is less than 1 (<1.68 g/L). Indeed, a low dose of AC@Fe causes a low production of hydroxyl radicals despite a significant amount of  $H_2O_2$  is added. While the number of active sites is insufficient to produce the hydroxyl radicals, the  $H_2O_2$  molecules react directly with the organic compounds in an incomplete oxidation process. Furthermore, for  $H_2O_2$  doses close to the

optimum, the removal efficiency of the TOC remains virtually constant despite the increase in the catalyst dose. This has been described by several authors as part of the  $H_2O_2$  molecules adsorbed on the surface of AC@Fe dispersed nanoparticles produces  $HO^\bullet$  radicals while other part is catalyzed by dissolved  $Fe^{2+}$  ions [25,57]. These adsorbed or  $HO^\bullet$  free radicals degrade and mineralize the organic pollutants also adsorbed or in solution up to their conversion into  $CO_2$  and  $H_2O$ . Otherwise, an overdose of  $H_2O_2$  ( $X_2 > 1$ , that is, greater than 25.2 mM) in the presence of a large amount of catalyst ( $X_1 > 1$ , that is, greater than 1.68 g/L) tends to reduce the efficiency of the process according to the  $HO^\bullet$  radicals trapping phenomenon by AC@Fe solid particles [58]. Another reason that could also explain this slow evolution of the TOC reduction rate is the production of hydroperoxyl radicals ( $HO_2^\bullet$ ) on the one hand from the reaction between  $H_2O_2$  and  $HO^\bullet$  (Eqs. (12) and (13)) [20,27] and on the other hand from the reaction between  $H_2O_2$  and  $Fe^{3+}$ (Eq. (14)) or AC@Fe<sup>III</sup> (Eq. (4)). Indeed, this production of  $HO_2^\bullet$  ( $E_0 = 1.7$  V) less oxidizing than the hydroxyl radicals ( $E_0 = 2.8$  V) is unfavorable to the oxidation of organic compounds.

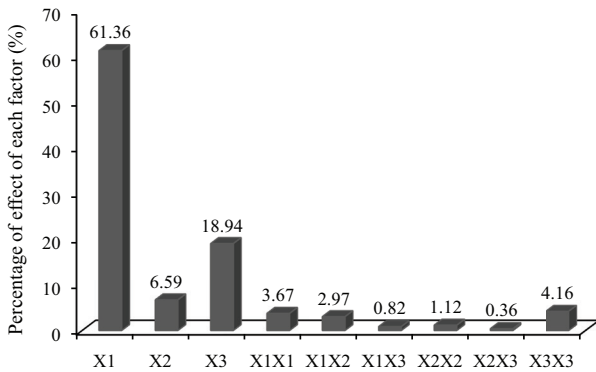
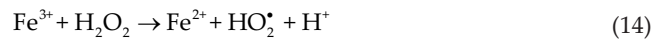


Fig. 4. Pareto graphical analysis of the effects of factors on TOC removal.

The optimal conditions would be in the range [1; 1.682] for  $X_1$  and [-1, 0] for  $X_2$  because the curves of isoresponse show that a reduction of 87.89% is possible for  $X_1 = 1.493$  and  $X_2 = -0.347$ .

A closer look at Fig. 6 shows a variety of responses reflecting the influence of the catalyst dose and initial TOC on the treatment process. For low TOC amounts, the TOC reduction rate increases gradually to high values reaching 90%. One of the reasons that may explain the ineffectiveness of the heterogeneous Fenton process for high TOC doses is the accessibility to the active sites of the catalyst by  $H_2O_2$ . In fact, the significant number of organic compounds or dyes present in the solution partially may obstruct the active sites of the catalyst. Therefore, the production of  $OH^\bullet$  radicals could be slowed down, thus affecting the catalytic performance of the Fenton process. For the catalyst, the value of  $X_1$  close to 1.682 undoubtedly yields to rates beyond 85%.

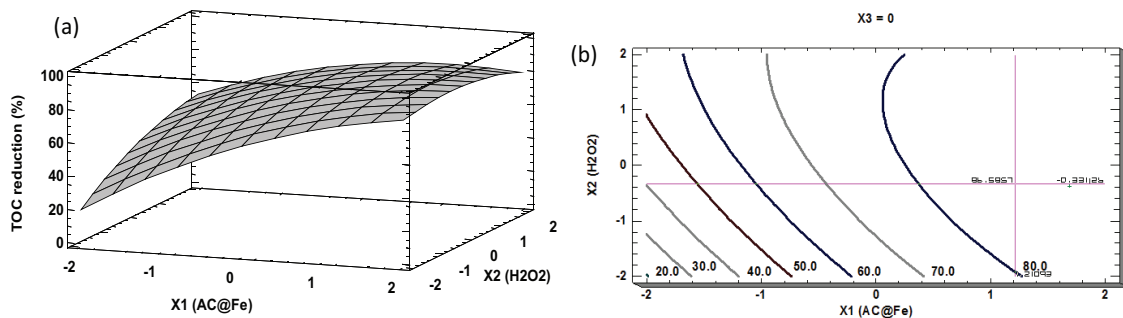


Fig. 5. Response surface (a) and contour plots (b) for TOC removal: effects of catalyst dosage and  $H_2O_2$  concentration.

Exceeding the lowest concentrations (i.e., for  $X_3$  in the range  $-1.682$  to  $-0.5$ ) is better to yield to approximately 90% of TOC reduction rate.

The analysis of Fig. 7 shows that the best TOC reduction rates are obtained for decreasing amounts of initial TOC and increasing amounts of  $H_2O_2$ . Indeed, high amounts of  $H_2O_2$  accelerate the production of hydroxyl radicals, capable to degrade organic compounds. However, a reasonable amount must be used to rationalize the reagents consumption and also for economic reasons. Thus, taking into consideration the isoresponse curves, the coded variable  $X_2$ , representing the amount of  $H_2O_2$ , must be between  $-0.5$  and  $0$  for the optimal treatment conditions. As  $X_3$  is in the range  $-1$  to  $-0.5$ , high abatement rates may be achieved for the initial TOC rate. In order to maximize the TOC concentration reduction, the initial conditions can be chosen within a limited experimental field having coded values in the range:  $[1, 1.682]$  for the amount of catalytic converter ( $X_1$ ),  $[-1, 0]$  for the amount of  $H_2O_2$  ( $X_2$ ), and  $[-1, -0.5]$  for initial TOC rate ( $X_3$ ).

Finally, using the “Statgraphics Centurion XVI” software [44], which integrates optimization mathematical functions, a 90.2% reduction in TOC is plausible under the following optimal experimental conditions:

- $X_1 = 1.682$  or 2 g/L of AC@Fe,
- $X_2 = -0.374$  or 16.73 mmol/L of  $H_2O_2$ ,
- $X_3 = -0.749$  or 99.83 mg/L of TOC initial.

3.2.2. Validation of the optimized conditions

Confirmatory tests were performed three times to confirm the optimized conditions predicting a 90.2% TOC rate

abatement (Table 5). Fenton degradation was studied at 32°C for 15 h in 50 mL of wastewater at 99.83 mg/L initial TOC containing 2 g/L of catalyst and 16.73 mmol/L of  $H_2O_2$ . Thus  $(90.40 \pm 1.04)\%$  TOC removal was obtained for the confirmatory test. This result is consistent with the rate of TOC removal under optimal conditions predicted by the model. At the same time, two tests were conducted, namely the adsorption on AC@Fe (in the absence of  $H_2O_2$ ) and the oxidation with only  $H_2O_2$ , in the same concentration, temperature and duration conditions as given above. The two reference tests have yielded TOC reduction rates of 53.2% for the adsorption on AC@Fe and 5.8% for the oxidation with  $H_2O_2$ , respectively. In light of the results, the heterogeneous Fenton process produces a sharp reduction in TOC concentration through the degradation of the organic compounds. The performance of the process depends on the adsorption capacity of the pollutants on the catalyst because the degradation happens at the external surface [59,60].

3.3. Kinetics of TOC degradation and spectral variation

Moreover, the UV-visible spectra of the residual solutions resulting from the different treatment processes under the optimal conditions have confirmed the dyes degradation (Fig. 8). The spectrum of the raw effluent presents three peaks at 227, 260 and 280 nm which reveal the presence of aromatic rings [37]. All these peaks have disappeared after Fenton treatment while their intensities have decreased after the reference tests. UV-visible spectral variations have confirmed the dyes degradation.

The kinetics of the different reactions studied by analyzing the TOC abatement rate (Fig. 9) shows two stages in the evolution of the degradation of the organic compounds of

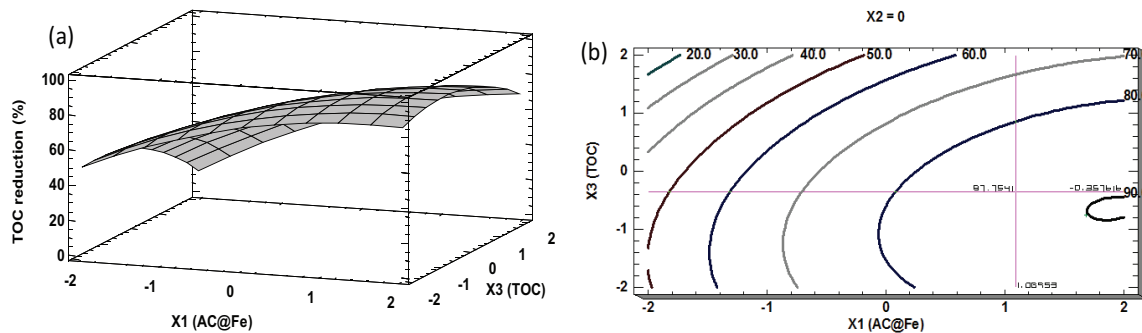


Fig. 6. Response surface (a) and contour plots (b) for TOC removal: effects of catalyst dosage and initial TOC.

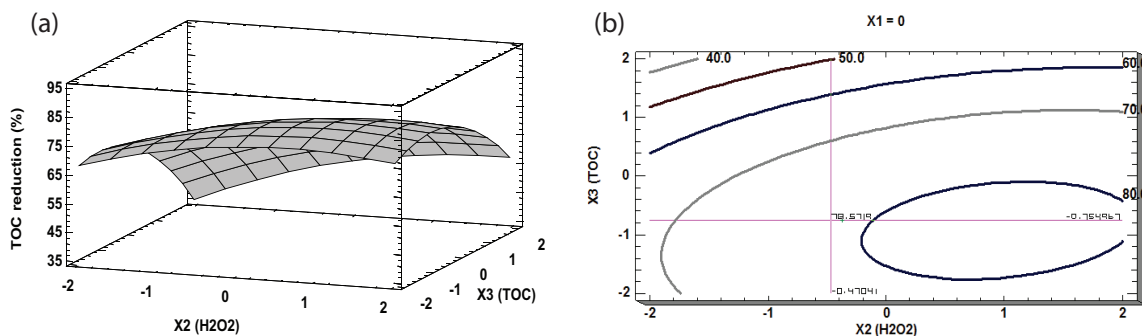


Fig. 7. Response surface (a) and contour plots (b) for TOC removal: effects of  $H_2O_2$  concentration and initial TOC.

Table 5  
Validation experiments at optimal operational conditions

	Optimum conditions		Responses		
	Catalyst dosage (g/L)	H <sub>2</sub> O <sub>2</sub> concentration (mM)	Initial TOC (mg/L)	Predicted (%)	Observed (%)
Heterogeneous Fenton	2	16.73	99.83	90.2	90.4
Adsorption	2		99.83		53.2
Oxidation		16.73	99.83		5.8

the effluent. The first step is characterized by a rapid TOC abatement rate (about 76%) after 2 h as previously reported for the heterogeneous Fenton process [61,62]. At the same time, 37.6% reduction of TOC was achieved by the adsorption process (AC@Fe) against 3.6% by direct oxidation with H<sub>2</sub>O<sub>2</sub>. The low oxidation potential of organic compounds by H<sub>2</sub>O<sub>2</sub> alone and the ability of AC@Fe to adsorb pollutants have shown that the success of AC@Fe/H<sub>2</sub>O<sub>2</sub> is due to adsorbed or free OH<sup>•</sup>. These results confirm the synergy between the iron oxide nanoparticles on the surface of the AC@Fe catalyst and H<sub>2</sub>O<sub>2</sub> for the improvement of TOC reduction over time. Indeed, the organic pollutants and H<sub>2</sub>O<sub>2</sub> are easily adsorbed on the AC@Fe active sites to initiate the heterogeneous catalytic oxidation reaction in order to accelerate the degradation process [57]. After this step, the degradation kinetics of organic compounds consisting mainly of intermediate compounds is very slow [63]. Indeed, Ramirez et al. [40] have argued that intermediate compounds are very resistant. In addition, the deactivation of the active sites could prevent the production of hydroxyl radicals which could be trapped in the degradation sludge.

### 3.4. Reusability and stability of catalyst

The AC@Fe catalytic performance was determined on five cycles of use by measuring the TOC reduction of the textile effluent and the iron leaching. Indeed, after each cycle, the reaction mixture was placed in an oven at 40°C for 10 h to accelerate the regeneration of the catalyst active sites and was then filtered to recover the catalyst. The catalyst particles were further washed with distilled water and dried in an oven for 2 h at 105°C. According to Fig. 10, a decrease in the efficiency of the TOC reduction rate was observed from the first cycle to the fifth cycle. Specifically, after the first cycle, a decrease in the catalytic efficiency of about 5% was observed in the second cycle. This could be explained by the loss of iron nanoparticles estimated at 0.53 mg/L after the first cycle. This loss is attributed to the dissolution of iron nanoparticles weakly bonded to the activated carbon surface. From the 2nd cycle, the efficiency turns from 84.6% to 78.7%, proving that the catalyst can be used up to the 5th cycle. This stability is attributed to the presence of iron nanoparticles accommodated and in the pores of the activated carbon (AC) and chemically bonded to the AC surface because only a low iron leaching (<0.15 mg Fe/L) was observed on all last four cycles. In addition, this amount of iron dissolved in the treated effluent would not be a source of surface water pollution because the cumulative iron ion content over all five cycles does not exceed 3 mg/L [64]. Finally, the use of AC@Fe could be worthwhile and effective for the depollution of real textile wastewater by Fenton process due to its catalytic stability.

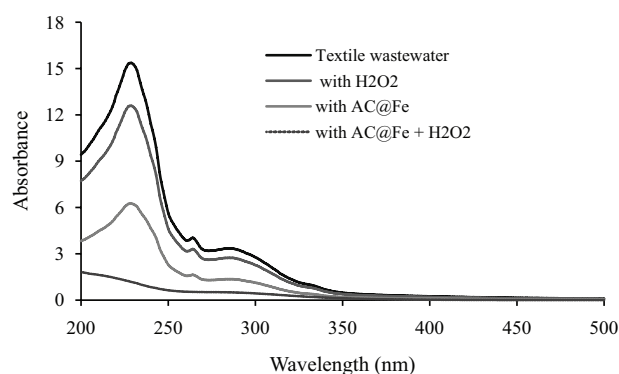


Fig. 8. Evaluation of the textile effluent spectra before and after 15 h of treatment.

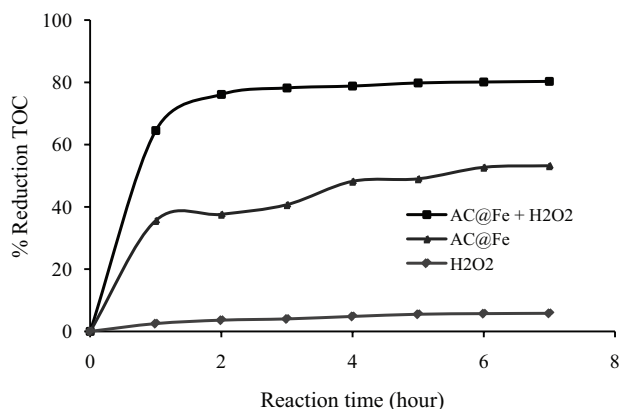


Fig. 9. TOC reduction kinetics of the textile effluent for different treatments.

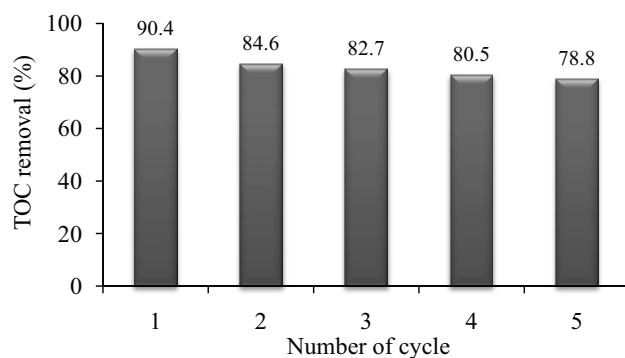


Fig. 10. Reuse of AC@Fe for the reduction of TOC of the textile effluent by the heterogeneous Fenton process under optimal conditions (H<sub>2</sub>O<sub>2</sub>: 16.73 mM; AC@Fe: 2 g/L; initial TOC: 99.83 mgC/L; pH: 4.0; temperature: 30°C; reaction time: 15 h).

### 3.5. Biodegradability of wastewater treated

Although the reduction of TOC is remarkable under optimal conditions, it is important to understand the subsequent biodegradation of the intermediate organic compounds contained in the treated effluent. For this purpose, three factors such as the BOD/COD ratio, the AOS and the COS were used as biodegradability indicators. AOS and COS can take values between +4 for  $\text{CO}_2$ , the most oxidized state of C, and -4 for  $\text{CH}_4$ , the lowest state of C. Indeed, AOS and COS are defined to evaluate the degree of oxidation and the efficiency of the oxidative process according to the equations proposed by Ahmadi et al. [64] (Eqs. (15) and (16)):

$$\text{AOS} = 4 - 1.5 \left( \frac{\text{COD}}{\text{TOC}} \right) \quad (15)$$

$$\text{COS} = 4 - 1.5 \left( \frac{\text{COD}}{\text{TOC}_i} \right) \quad (16)$$

where COD is the chemical oxygen demand ( $\text{mg O}_2/\text{L}$ ) at time  $t$  (h), TOC is total organic carbon ( $\text{mg/L}$ ) at time  $t$  (h) and  $\text{TOC}_i$  is initial total organic carbon ( $\text{mg/L}$ ). Before the COD

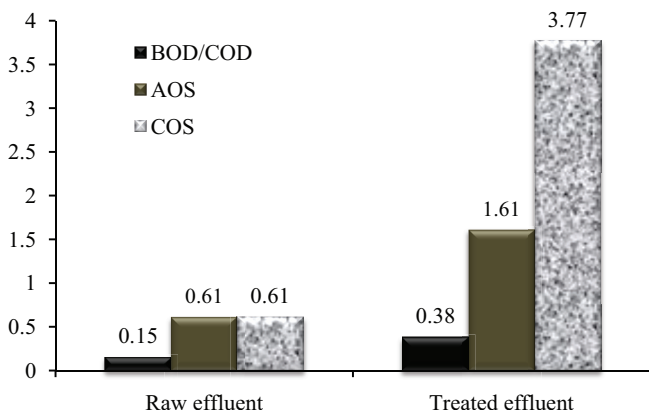


Fig. 11. Main biodegradability indices before and after treatment of the textile effluent by the heterogeneous Fenton process (15 h) under optimal conditions.

Table 6

Efficiency of the AC@Fe catalyst from present study compared with other works on the depollution of real wastewater by the heterogeneous Fenton process

	Catalyst dose (g/L)	pH	$\text{H}_2\text{O}_2$ (mM)	COD (mg/L)	TOC (mg/L)	Time (h)	Efficiency (%)	References
Textile wastewater	AC/Fe: 300	3	14.7	1,000		24	70	[63]
Landfill leachate	Fe-C: 55.7	3	157.6	4,980		60	74.6	[29]
Petrochemical wastewater	MNPs@C: 1	3	50	50–1,000	250–300	4	86	[27]
Textile wastewater	AC@Fe: 2	4	16.73	225.4	99.8	15	90.4	Present study

analysis, the pH of the water sample was adjusted to the basic pH to avoid the overestimation of COD by the residual  $\text{H}_2\text{O}_2$  in solution.

Thus, after 15 h of treatment under optimal conditions, these biodegradability indicators are reported in Fig. 11. The BOD/COD ratio of the raw effluent, which was 0.15, has reached 0.38 for the treated effluent, showing a significant improvement in the biodegradability of the effluent. This has demonstrated the presence of simple organic compounds in the treated effluent that are easy to biodegrade. In addition, the higher AOS and COS values of the treated effluent than those of the raw one have confirmed its high level of biodegradability. Indeed, Souza et al. [65], then Ahmadi et al. [64] reported that the increase in AOS and COS values indicates the efficiency of the oxidation process. Thus, the use of the AC@Fe catalyst for the treatment of this textile effluent by the heterogeneous Fenton process under optimal conditions made it possible to degrade the refractory organic compounds into highly biodegradable intermediate compounds.

### 3.6. Comparison of the depollution efficiency

Our study was compared with previous works on the treatment of real wastewater by the heterogeneous Fenton process using iron nanoparticles supported on activated carbon. Thus, under optimal experimental conditions (Table 6), Kakavandi and Babaei [27] removed 86% of COD from the petrochemical wastewater; Wang et al. [29] obtained 74.6% COD removal of landfill leachate, and Dantas et al. [63] removed 70% of COD from the textile wastewater. The degradation efficiency was evaluated in terms of COD whereas this parameter takes into account only the oxidizable organic compounds by potassium dichromate. In this present study, depollution has been measured by the TOC reduction rate, which is a parameter evaluating all organic matter. Therefore, this study appears satisfactory.

## 4. Conclusion

The efficiency of the RSM based on the central composite design has been demonstrated for the optimization of the treatment conditions of a real textile wastewater from Bamako handicraft loincloths dyeing by the heterogeneous Fenton process. The results of the analysis of variance showed that the regression model can be used to predict the TOC concentration

reduction of a textile effluent from initial experimental conditions. Thus, using the predicted optimal conditions such as catalyst dose (2 g/L), H<sub>2</sub>O<sub>2</sub> dose (16.73 mmol/L) and initial TOC concentration (99.83 mgC/L), a 90.4% experimental TOC reduction has been measured, while the model predicted a 90.2% TOC rate reduction. This high abatement yield is partly attributed to the heterogeneous Fenton process using iron oxide (FeO) nanoparticles supported on an activated carbon prepared from a banana spike. Their homogeneous dispersion on the surface of the activated carbon and their location inside the internal porosity of AC, strongly contributed to the reduction of TOC as revealed by the Pareto analysis.

### Acknowledgments

The authors are grateful for the financial support provided by the “Agence Française de la Francophonie” (AUF), the French Embassy of Ivory Coast and Campus, France, which funded the grants of Bi Gouessé Henri Briton.

### References

- [1] M. El Bouraie, W.S. El Din, Biodegradation of Reactive Black 5 by *Aeromonas hydrophila* strain isolated from dye-contaminated textile wastewater, *Sustain. Environ. Res.*, 26 (2016) 209–216.
- [2] M. Rajasimman, S.V. Babu, N. Rajamohan, Biodegradation of textile dyeing industry wastewater using modified anaerobic sequential batch reactor – start-up, parameter optimization, *J. Taiwan Inst. Chem. Eng.*, 72 (2017) 1–11.
- [3] T.K.F.S. Freitas, V.M. Oliveira, M.T.F. de Souza, H.C.L. Geraldino, V.C. Almeida, S.L. Fávoro, J.C. Garcia, Optimization of coagulation-flocculation process for treatment of industrial textile wastewater using okra (*A. esculentus*) mucilage as natural coagulant, *Ind. Crops Prod.*, 76 (2015) 538–544.
- [4] G. Han, C.Z. Liang, T.S. Chung, M. Weber, C. Staudt, C. Maletzko, Combination of forward osmosis (FO) process with coagulation/flocculation (CF) for potential treatment of textile wastewater, *Water Res.*, 91 (2016) 361–370.
- [5] F. Duarte, V. Morais, F.J. Maldonado-Hódar, L.M. Madeira, Treatment of textile effluents by the heterogeneous Fenton process in a continuous packed-bed reactor using Fe/activated carbon as catalyst, *Chem. Eng. J.*, 232 (2013) 34–41.
- [6] J.P. Guin, Y.K. Bhardwaj, L. Varshney, Mineralization and biodegradability enhancement of Methyl Orange dye by an effective advanced oxidation process, *Appl. Radiat. Isot.*, 122 (2017) 153–157.
- [7] M. Luan, G. Jing, Y. Piao, D. Liu, L. Jin, Treatment of refractory organic pollutants in industrial wastewater by wet air oxidation, *Arab. J. Chem.*, 10 (2017) 769–776.
- [8] A. Rodríguez, G. Ovejero, M.D. Romero, C. Díaz, M. Barreiro, J. García, Catalytic wet air oxidation of textile industrial wastewater using metal supported on carbon nanofibers, *J. Supercrit. Fluids*, 46 (2008) 163–172.
- [9] Sushma, A.K. Saroha, Treatment of industrial organic raffinate containing pyridine and its derivatives by coupling of catalytic wet air oxidation and biological processes, *J. Clean. Prod.*, 162 (2017) 973–981.
- [10] F. Torrades, J. García-Montaña, Using central composite experimental design to optimize the degradation of real dye wastewater by Fenton and photo-Fenton reactions, *Dyes Pigm.*, 100 (2014) 184–189.
- [11] M.R. Taha, A.H. Ibrahim, COD removal from anaerobically treated palm oil mill effluent (AT-POME) via aerated heterogeneous Fenton process: optimization study, *J. Water Proc. Eng.*, 1 (2014) 8–16.
- [12] Y. Yao, L. Wang, L. Sun, S. Zhu, Z. Huang, Y.M. WangyangLu, W. Chen, Efficient removal of dyes using heterogeneous Fenton catalysts based on activated carbon fibers with enhanced activity, *Chem. Eng. Sci.*, 101 (2013) 424–431.
- [13] P.V. Nidheesh, Heterogeneous Fenton catalysts for the abatement of organic pollutants from aqueous solution: a review, *RSC Adv.*, 5 (2015) 40552–40577.
- [14] S. Cheng, L. Zhang, H. Xia, J. Peng, S. Zhang, S. Wang, Preparation of high specific surface area activated carbon from walnut shells by microwave-induced KOH activation, *J. Porous Mater.*, 22 (2015) 1527–1537.
- [15] P.P. Gan, S.F.Y. Li, Efficient removal of Rhodamine B using a rice hull-based silica supported iron catalyst by Fenton-like process, *Chem. Eng. J.*, 229 (2013) 351–363.
- [16] Y. Zhang, J. Shang, Y. Song, C. Rong, Y. Wang, W. Huang, K. Yu, Selective Fenton-like oxidation of methylene blue on modified Fe-zeolites prepared via molecular imprinting technique, *Water Sci. Technol.*, 75 (2017) 659–669.
- [17] W. Li, D. Wan, G. Wang, K. Chen, Q. Hu, L. Lu, Heterogeneous Fenton degradation of Orange II by immobilization of Fe<sub>3</sub>O<sub>4</sub> nanoparticles onto Al-Fe pillared bentonite, *Korean J. Chem. Eng.*, 33 (2016) 1557–1564.
- [18] S.H. Yoo, D. Jang, H.-I. Joh, S. Lee, Iron oxide/porous carbon as a heterogeneous Fenton catalyst for fast decomposition of hydrogen peroxide and efficient removal of methylene blue, *J. Mater. Chem. A*, 5 (2017) 748–755.
- [19] C. Yaman, G. Gündüz, A parametric study on the decolorization and mineralization of C.I. Reactive Red 141 in water by heterogeneous Fenton-like oxidation over FeZSM-5 zeolite, *J. Environ. Health Sci. Eng.*, 13 (2015) 1–12.
- [20] A. Khataee, F. Salahpour, M. Fathinia, B. Seyyedi, B. Vahid, Iron rich laterite soil with mesoporous structure for heterogeneous Fenton-like degradation of an azo dye under visible light, *J. Ind. Eng. Chem.*, 26 (2015) 129–135.
- [21] X. Hou, X. Huang, F. Jia, Z. Ai, J. Zhao, L. Zhang, Hydroxylamine promoted goethite surface Fenton degradation of organic pollutants, *Environ. Sci. Technol.*, 51 (2017) 5118–5126.
- [22] H. Guedidi, L. Reinert, Y. Soneda, N. Bellakhal, L. Duclaux, Adsorption of ibuprofen from aqueous solution on chemically surface-modified activated carbon cloths, *Arabian J. Chem.*, 10 (2017) S3584–S3594.
- [23] M. Jaouadi, S. Hbaieb, H. Guedidi, L. Reinert, N. Amdouni, L. Duclaux, Preparation and characterization of carbons from  $\beta$ -cyclodextrin dehydration and from olive pomace activation and their application for boron adsorption, *J. Saudi Chem. Soc.*, 21 (2017) 822–829.
- [24] F.G. de Mendonça, M.G. Rosmaninho, P.X. da Fonseca, R.R. Soares, J.D. Ardisson, J.C. Tristão, R.M. Lago, Use of iron and bio-oil wastes to produce highly dispersed Fe/C composites for the photo-Fenton reaction, *Environ. Sci. Pollut. Res.*, 24 (2017) 6151–6156.
- [25] M. Ahmadi, B. Kakavandi, S. Jorfi, M. Azizi, Oxidative degradation of aniline and benzotriazole over PAC@Fe<sup>II</sup>Fe<sup>III</sup>O<sub>4</sub>: a recyclable catalyst in a heterogeneous photo-Fenton-like system, *J. Photochem. Photobiol., A*, 336 (2017) 42–53.
- [26] C.S. Castro, M.C. Guerreiro, L.C. a Oliveira, M. Gonçalves, a.S. Anastácio, M. Nazzarro, Iron oxide dispersed over activated carbon: support influence on the oxidation of the model molecule methylene blue, *Appl. Catal. A*, 367 (2009) 53–58.
- [27] B. Kakavandi, A.A. Babaei, Heterogeneous Fenton-like oxidation of petrochemical wastewater using a magnetically separable catalyst (MNPs@C): process optimization, reaction kinetics and degradation mechanisms, *RSC Adv.*, 6 (2016) 84999–85011.
- [28] Y. Kan, Q. Yue, D. Li, Y. Wu, B. Gao, Preparation and characterization of activated carbons from waste tea by H<sub>3</sub>PO<sub>4</sub> activation in different atmospheres for oxytetracycline removal, *J. Taiwan Inst. Chem. Eng.*, 71 (2017) 494–500.
- [29] L. Wang, Q. Yang, D. Wang, X. Li, G. Zeng, Z. Li, Y. Deng, J. Liu, K. Yi, Advanced landfill leachate treatment using iron-carbon microelectrolysis-Fenton process: process optimization and column experiments, *J. Hazard. Mater.*, 318 (2016) 460–467.
- [30] B. Yang, Z. Tian, L. Zhang, Y. Guo, S. Yan, Enhanced heterogeneous Fenton degradation of Methylene Blue by nanoscale zero valent iron (nZVI) assembled on magnetic Fe<sub>3</sub>O<sub>4</sub>/reduced graphene oxide, *J. Water Proc. Eng.*, 5 (2015) 101–111.
- [31] S. Cheng, J. Wu, H. Xia, J. Peng, S. Wang, L. Zhang, Microwave-assisted regeneration of spent activated carbon from paracetamol

- wastewater plant using response surface methodology, *Desal. Wat. Treat.*, 57 (2016) 18981–18991.
- [32] K. Salehi, A. Bahmani, B. Shahmoradi, M.A. Pordel, S. Kohzadi, Y. Gong, H. Guo, H.P. Shivaraju, R. Rezaee, R.R. Pawar, S.-M. Lee, Response surface methodology (RSM) optimization approach for degradation of Direct Blue 71 dye using CuO-ZnO nanocomposite, *Int. J. Environ. Sci. Technol.*, 14 (2017) 2067–2076.
- [33] N. Biglarjoo, S.A. Mirbagheri, M. Ehteshami, S.M. Ghaznavi, Optimization of Fenton process using response surface methodology and analytic hierarchy process for landfill leachate treatment, *Process. Saf. Environ. Prot.*, 104 (2016) 150–160.
- [34] M.O. Saeed, K. Azizli, M.H. Isa, M.J.K. Bashir, Application of CCD in RSM to obtain optimize treatment of POME using Fenton oxidation process, *J. Water Proc. Eng.*, 8 (2015) 7–16.
- [35] P. Sugumaran, V.P. Susan, P. Ravichandran, S. Seshadri, Production and Characterization of Activated Carbon from Banana Empty Fruit Bunch and Delonix regia Fruit Pod, *J. Sustain. Energy Environ.*, 3 (2012) 125–132.
- [36] T. Kuokkanen, P. Vähöja, I. Välimäki, R. Lauhanen, Suitability of the respirometric Bod oxitop method for determining the biodegradability of oils in ground water using forestry hydraulic oils as model compounds, *Int. J. Environ. Anal. Chem.*, 84 (2004) 677–689.
- [37] T.D. Nguyen, N.H. Phan, M.H. Do, K.T. Ngo, Magnetic Fe<sub>2</sub>MO<sub>4</sub> (M:Fe, Mn) activated carbons: Fabrication, characterization and heterogeneous Fenton oxidation of methyl orange, *J. Hazard. Mater.*, 185 (2011) 653–661.
- [38] T. Van Thuan, B.T.P. Quynh, T.D. Nguyen, V.T.T. Ho, L.G. Bach, Response surface methodology approach for optimization of Cu<sup>2+</sup>, Ni<sup>2+</sup> and Pb<sup>2+</sup> adsorption using KOH-activated carbon from banana peel, *Surf. Interfaces*, 6 (2017) 209–217.
- [39] M. Gao, D. Zhang, W. Li, J. Chang, Q. Lin, D. Xu, H. Ma, Degradation of methylene blue in a heterogeneous Fenton reaction catalyzed by chitosan crosslinked ferrous complex, *J. Taiwan Inst. Chem. Eng.*, 67 (2016) 355–361.
- [40] J.H. Ramirez, F.J. Maldonado-Hódar, A.F. Pérez-Cadenas, C. Moreno-Castilla, C.A. Costa, L.M. Madeira, Azo-dye Orange II degradation by heterogeneous Fenton-like reaction using carbon-Fe catalysts, *Appl. Catal., B*, 75 (2007) 312–323.
- [41] L. Núñez, J.A. García-Hortal, F. Torrades, Study of kinetic parameters related to the decolorization and mineralization of reactive dyes from textile dyeing using Fenton and photo-Fenton processes, *Dyes Pigm.*, 75 (2007) 647–652.
- [42] F. Torrades, S. Saiz, J.A. García-Hortal, Using central composite experimental design to optimize the degradation of black liquor by Fenton reagent, *Desalination*, 268 (2011) 97–102.
- [43] H. Aghdasinia, R. Bagheri, B. Vahid, A. Khataee, Central composite design optimization of pilot plant fluidized-bed heterogeneous Fenton process for degradation of an azo dye, *Environ. Technol. (United Kingdom)*, 37 (2016) 2703–2712.
- [44] J.R. Domínguez, T. González, P. Palo, E.M. Cuerda-Correa, Fenton + Fenton-like integrated process for carbamazepine degradation: optimizing the system, *Ind. Eng. Chem. Res.*, 51 (2012) 2531–2538.
- [45] K.S.W. Sing, D.H. Everett, R.A.W. Haul, L. Moscou, R.S. Pierotti, J. Rouquerol, T. Siemieniowska, International Union of Pure Commission on Colloid and Surface Chemistry Including Catalysis-Reporting physisorption data for gas/solid systems with special reference to the determination of surface area and porosity, *Pure Appl. Chem.*, 57 (1985) 603–619.
- [46] M. Delarmelina, S.J. Greco, J.W. d. M. Carneiro, Single step mechanism for nucleophilic substitution of 2,3-dichloro naphthoquinone using nitrogen, oxygen and sulfur nucleophiles: a DFT approach, *Tetrahedron*, 73 (2017) 4363–4370.
- [47] S. Bhattacharya, R. Rahaman, S. Chatterjee, T.K. Paine, Aliphatic C–C bond cleavage in  $\alpha$ -hydroxy ketones by a dioxygen-derived nucleophilic iron-oxygen oxidant, *Chem. Eur. J.*, 23 (2017) 3815–3818.
- [48] P. Manechakr, S. Karnjanakom, Adsorption behaviour of Fe(II) and Cr(VI) on activated carbon: surface chemistry, isotherm, kinetic and thermodynamic studies, *J. Chem. Thermodyn.*, 106 (2017) 104–112.
- [49] O. Beswick, I. Yuranov, D.T.L. Alexander, L. Kiwi-Minsker, Iron oxide nanoparticles supported on activated carbon fibers catalyze chemoselective reduction of nitroarenes under mild conditions, *Catal. Today*, 249 (2015) 45–51.
- [50] B. Kakavandi, A. Takdastan, N. Jaafarzadeh, M. Azizi, A. Mirzaei, A. Azari, Application of Fe<sub>3</sub>O<sub>4</sub>@C catalyzing heterogeneous UV-Fenton system for tetracycline removal with a focus on optimization by a response surface method, *J. Photochem. Photobiol., A*, 314 (2016) 178–188.
- [51] S. Gota, E. Guiot, M. Henriot, M. Gautier-Soyer, Atomic-oxygen-assisted MBE growth of  $\alpha$ -Fe<sub>2</sub>O<sub>3</sub> on  $\alpha$ -Al<sub>2</sub>O<sub>3</sub>(0001): Metastable FeO(111)-like phase at subnanometer thicknesses, *Phys. Rev. B*, 60 (1999) 14387–14395.
- [52] W. Han, S. Huang, T. Cheng, H. Tang, Y. Li, H. Liu, Applied Surface Science Promotion of Nb<sub>2</sub>O<sub>5</sub> on the wustite-based iron catalyst for ammonia synthesis, *Appl. Surf. Sci.*, 353 (2015) 17–23.
- [53] I. Sapkaite, E. Barrado, F. Fdz-Polanco, S.I. Pérez-Elvira, Optimization of a thermal hydrolysis process for sludge pre-treatment, *J. Environ. Manage.*, 192 (2017) 25–30.
- [54] J. Xu, Y. Long, D. Shen, H. Feng, T. Chen, Optimization of Fenton treatment process for degradation of refractory organics in pre-coagulated leachate membrane concentrates, *J. Hazard. Mater.*, 323 (2017) 674–680.
- [55] M.A. Rauf, N. Marzouki, B.K. Körbahti, Photolytic decolorization of Rose Bengal by UV/H<sub>2</sub>O<sub>2</sub> and data optimization using response surface method, *J. Hazard. Mater.*, 159 (2008) 602–609.
- [56] T. Xu, Y. Liu, F. Ge, L. Liu, Y. Ouyang, Application of response surface methodology for optimization of azocarmine B removal by heterogeneous photo-Fenton process using hydroxy-iron-aluminum pillared bentonite, *Appl. Surf. Sci.*, 280 (2013) 926–932.
- [57] A.A. Babaei, B. Kakavandi, M. Rafiee, F.K. Kalantar Hormozi, I. Purkaram, E. Ahmadi, S. Esmaili, Comparative treatment of textile wastewater by adsorption, Fenton, UV-Fenton and US-Fenton using magnetic nanoparticles-functionalized carbon (MNP@C), *J. Ind. Eng. Chem.*, 56 (2017) 163–174.
- [58] O.B. Ayodele, H.S. Auta, N. Md Nor, Artificial neural networks, optimization and kinetic modeling of amoxicillin degradation in photo-fenton process using aluminum pillared montmorillonite-supported ferrioxalate catalyst, *Ind. Eng. Chem. Res.*, 51 (2012) 16311–16319.
- [59] A. Jonidi Jafari, B. Kakavandi, N. Jaafarzadeh, R. Rezaei Kalantary, M. Ahmadi, A. Akbar Babaei, Fenton-like catalytic oxidation of tetracycline by AC@Fe<sub>3</sub>O<sub>4</sub> as a heterogeneous persulfate activator: adsorption and degradation studies, *J. Ind. Eng. Chem.*, 45 (2017) 323–333.
- [60] X. Liu, H. Yin, A. Lin, Z. Guo, Effective removal of phenol by using activated carbon supported iron prepared under microwave irradiation as a reusable heterogeneous Fenton-like catalyst, *J. Environ. Chem. Eng.*, 5 (2017) 870–876.
- [61] J.A. Zazo, J.A. Casas, A.F. Mohedano, J.J. Rodríguez, Catalytic wet peroxide oxidation of phenol with a Fe/active carbon catalyst, *Appl. Catal., B*, 65 (2006) 261–268.
- [62] N. Barhoumi, H. Olvera-Vargas, N. Oturan, D. Huguenot, A. Gadri, S. Ammar, E. Brillas, M.A. Oturan, Kinetics of oxidative degradation/mineralization pathways of the antibiotic tetracycline by the novel heterogeneous electro-Fenton process with solid catalyst chalcocopyrite, *Appl. Catal., B*, 209 (2017) 637–647.
- [63] T.L.P. Dantas, V.P. Mendonça, H.J. José, A.E. Rodrigues, R.F.P.M. Moreira, Treatment of textile wastewater by heterogeneous Fenton process using a new composite Fe<sub>2</sub>O<sub>3</sub>/carbon, *Chem. Eng. J.*, 118 (2006) 77–82.
- [64] M. Ahmadi, B. Kakavandi, N. Jaafarzadeh, A. Akbar Babaei, Catalytic ozonation of high saline petrochemical wastewater using PAC@Fe<sup>II</sup>Fe<sup>III</sup>O<sub>4</sub>: Optimization, mechanisms and biodegradability studies, *Sep. Purif. Technol.*, 177 (2017) 293–303.
- [65] B.S. Souza, F.C. Moreira, M.W.C. Dezotti, V.J.P. Vilar, R.A.R. Boaventura, Application of biological oxidation and solar driven advanced oxidation processes to remediation of winery wastewater, *Catal. Today*, 209 (2013) 201–208.